Electronic Supplementary Information

Thermally Stable, Planar Hybrid Perovskite Solar Cells with High Efficiency

Kyoungwon Choi,‡ Junwoo Lee,‡ Hong Il Kim, Cheol Woong Park, Guan-Woo Kim, Hyuntae Choi, Sungjin Park, Sang Ah Park and Taiho Park*

[*] Prof. Taiho Park. Corresponding-Author: E-mail: taihopark@postech.ac.kr

[‡] There authors are contributed equally to this manuscript.

Department of Chemical Engineering, Pohang University of Science and Technology (POSTECH), 77 Cheongam-Ro, Nam-gu, Pohang, Gyeongbuk, Republic of Korea. Fax: +82-54-279-8298; Tel: +82-54-279-2394

Contents

Experimental details

Fig. S1 Chemical structures of the 3-(1-Pyridinio)-1-propanesulfonate used in this study and ESP map of the zwitterion.

Fig. S2 XPS survey spectrum of SnO_2.

Fig. S3 XPS high resolution spectra of SnO_2 and Zw-SnO_2 for Sn 3d, respectively.

Fig. S4 Absorption spectra of SnO_2 and Zw-SnO_2, respectively. Insets: Corresponding Tauc plots for bandgap extraction.

Fig. S5 (a) NEXAFS PEY mode of Zw-SnO_2. (b) Intensities of π* transitions vs incidence angle.

Fig. S6 (a) *I*–*V* characteristics of FTO/SnO_2/Au, FTO/SnO_2/PEIE/Au, FTO/SnO_2/IL/Au and FTO/SnO_2/zwitterion/Au devices, respectively. (b) SEM images of each ETLs with different interlayers, respectively.

Fig. S7 (a) Contact angle images of each ETL using glycerol and DI water, respectively. (b) Contact angle values and surface energies of each ETL.

Fig. S8 Top-view SEM images of perovskite films on the SnO_2 and Zw-SnO_2, respectively.

Fig. S9 Normalized absorbance at 700nm for perovskite films on the SnO_2 and Zw-SnO_2, respectively.

Fig. S10 Cross-sectional SEM images of the SnO_2 and Zw-SnO_2-based samples under heat treatment at 150°C.

Fig. S11 PCE of the SnO_2 and Zw-SnO_2-based device as a function of time under 1 sun illumination.

Fig. S12 IPCE measurement and integrated J_{SC} of (a) SnO_2, Zw-SnO_2 and (b) CBD-Zw-SnO_2 device, respectively.

Fig. S13 J_{SC} dependence on light intensity.

Fig. S14 Optical microscope images of Zw-SnO_2 with different concentrations, respectively.

Fig. S15 Steady state photoluminescence (PL) spectra of the SnO_2 and the Zw-SnO_2, respectively.

Fig. S16 Equivalent circuit model for EIS measurement.

Fig. S17 Temperature-dependent thermal stability of SnO_2 and Zw-SnO_2-based devices, respectively.

Fig. S18 Time-dependent thermal stability of device based on different concentrations of zwitterion at 85°C, 85 % humidity.

Fig. S19 *J*–*V* curves of asy_PBTBDT_Zw-SnO2-based device.

Fig. S20 TGA curve of 3-(1-pyridinio)-1-propanesulfonate.

Fig. S21 Long-term stability test at 25°C, 25% humidity.

Table S1 Calculated parameters for the energy level of ETLs

Table S2 Calculated conductivities of each ETL with the different interlayers

Table S3 Photovoltaic parameters obtained from the best devices at each condition

Table S4 Summary of the electron lifetimes

Table S5 Slope of the Mott–Schottky plots and doping densities of ETLs

Table S6 Parameters of the equivalent circuit

Table S7 The initial absolute PCEs for SnO_2 and Zw-SnO2 devices

Table S8 Summary of device performances obtained from devices employing Spiro_SnO_2, Spiro_Zw-SnO_2, Polymer_SnO_2 and Polymer_Zw-SnO_2

Experimental details

1) Device characterization

The *J-V* curve and maximum power point efficiency (MPP) was measured by using Keithley 2400 SMU and an Oriel xenon lamp (450 W) with an AM1.5 filter. The solar cell performance was characterized under AM 1.5G illumination of 100 $mWcm^{-2}$ (Oriel 1 kW solar simulator), which was calibrated with a KG5 filter certified by NREL. The *J-V* curves of all devices were measured by reverse (1.2 V to -0.2 V) or forward (-0.2 V to 1.2 V) with 0.02 Vs^{-1} of scan rate. The active area of device is 0.09 cm^2. The MPP was measured under the maximum power point voltage. The conductivity of ETLs was calculated by following equation:

$$\sigma = /d\ /VA$$

where, *A* is the area (0.09 cm2) and *d* is the thickness of the samples.

2) IPCE measurement

Constant 100 W Xenon lamp source with an automated monochromator filters and 0.76 mm x 1.0 mm rectangular spot size was used for incident photon-to-current efficiency (IPCE) spectra. The measurements were conducted in the wavelength range from 300 to 1100 nm, chopped at 4 Hz (IQE-200B model).

3) PL measurement

Time-resolved photoluminescence (TRPL) mesurements were performed using time correlated single photon counting (TCSPC) system (HAMAMATSU/C11367-31). For TRPL measurements, a pulsed laser source was laser diode with a wavelength of 474 nm, a repetition rate of 100 kHz, fluence of ~ 4 nJ/cm^2 and a pulse width of 70 ps. Steady state photoluminescence (PL) measurements were performed using the high resolution monochromator and hybrid photomultiplier detector (PMA Hybrid 40, PicoQuant GmbH). The TRPL and steady-state PL measurements were conducted using prepared samples: glass/perovskite or glass/ETL/perovskite or FTO/ETL/perovskite. The samples were excited from the glass side under ambient conditions with excitation wavelength of 474nm. The PL decay constants were calculated using a bi-exponential equation:

$$f(t) = A_1 \exp(-\frac{t}{\tau_1}) + A_2 \exp(-\frac{t}{\tau_2}) + y_0$$

where, *A* is the decay amplitude, and τ is the decay time.

4) SEM measurement

Field emission scanning electron microscope (FE-SEM, Hitachi S 4800) was employed for the surface of the electron transport layers (ETLs).

5) UV-vis measurement

The Ultraviolet-visible (UV-vis) absorption spectra were obtained using a Mecasys Optizen Pop UV-vis spectrophotometer for FTO/SnO_2 and FTO/Zw-SnO_2.

6) UPS measurement

The UPS measurements were carried out using AXIS-NOVA and Ultra DLD (KRATOS Inc.) Mono-chromatic He I (21.22 eV) for UPS base pressure 2.0 x 10^{-9} Torr without surface treatment. UPS measurement

7) FT-IR measurement

The Fourier transform infrared spectra of SnO_2 and Zw-SnO_2 were measured using a Cary 600 spectrometer equipped with a MCT-A (mercury cadmium telluride) detector.

8) SCLC measurement

The device structure of FTO/ETL/perovskite/LiF/Al was measured using a Keithely 2400 SMU (0 V to 5V) to evaluate the trap densities of devices. The trap densities were calculated using the following equation:

$$V_{TFL} = \frac{en_t d^2}{2\varepsilon\varepsilon_0}$$

where V_{TFL} is the trap-filled limit voltage, e is the elementary charge, n_t is the trap density, d is the film thickness, ε is the dielectric constant, and ε_0 is the vacuum permittivity.

9) Contact angle measurement

Contact angle images were measured under white LED module. Di-water and glycerol were applied to calculate surface energy (the polar surface tension 50.7 mJm^{-2} for di-water, 1.8 mJm^{-2} for glycerol and the dispersion surface tension 22.1 mJm^{-2} for di-water, 49 mJm^{-2} for glycerol were used). The samples (FTO bare glass, SnO_2, Zw-SnO_2 substrates) were prepared with same process mentioned at solar cell fabrication.

10) Near-Edge X-Ray Absorption of Fine Structure (NEXAFS) and XPS measurement

NEXAFS and XPS measurements were performed at 4D PES beamline of PAL in Korea. We used the partial electron yield (PEY) detection mode for the NEXAFS spectra by recording the sample current normalized to a signal current.

11) Optical microscope measurement

The optical microscope images were measured using an Axioplan microscope (ZEISS).

12) Impedance measurement

The impedance of perovskite solar cells were measured using a computer-controlled potentiostat (SP-200, BioLogic). For FTO/ETL/perovskite/Spiro-OMeTAD/Au devices, electrochemical impedance spectroscopy (EIS) plot was measured in the frequency range of 1 MHz to 1 Hz in the dark condition under a bias of V_{OC}. The doping density was calculated using the Mott–Schottky equation, as follows:

$$\frac{1}{C^2} = \frac{2}{\varepsilon\varepsilon_0 e A^2 N}\left(V_{bi} - V\right)$$

where C is the capacitance, ε is dielectric constant, ε0 is the permittivity of free space, e is the elementary charge, A is the active area (0.09 cm2), N is the doping density of the semiconductor, and V is the applied bias.

13) XRD measurement

X-Ray diffraction analysis (XRD, Rigaku D/Max-2200/PC) was employed for perovskite crystal phase identification.

14) DFT calculation

Density Functional Theory (DFT) calculations were carried out to calculate the density of states of the perovskite crystal using the PWSCF program of the Quantum Espresso software package with a planewave/pseudopotential approach.[1]

15) TGA measurement

The TGA data were obtained under nitrogen atmosphere on a TGA Q50 anlayzer.

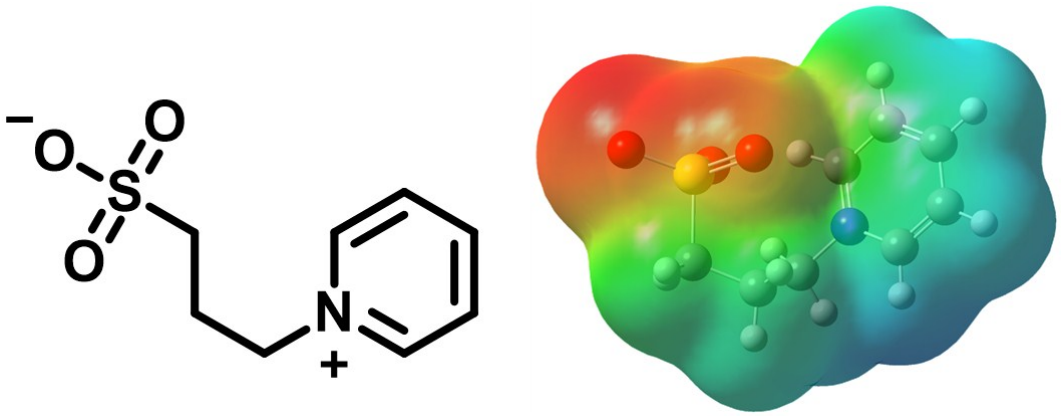

Fig. S1 Chemical structures of the 3-(1-Pyridinio)-1-propanesulfonate used in this study and ESP map of the zwitterion.

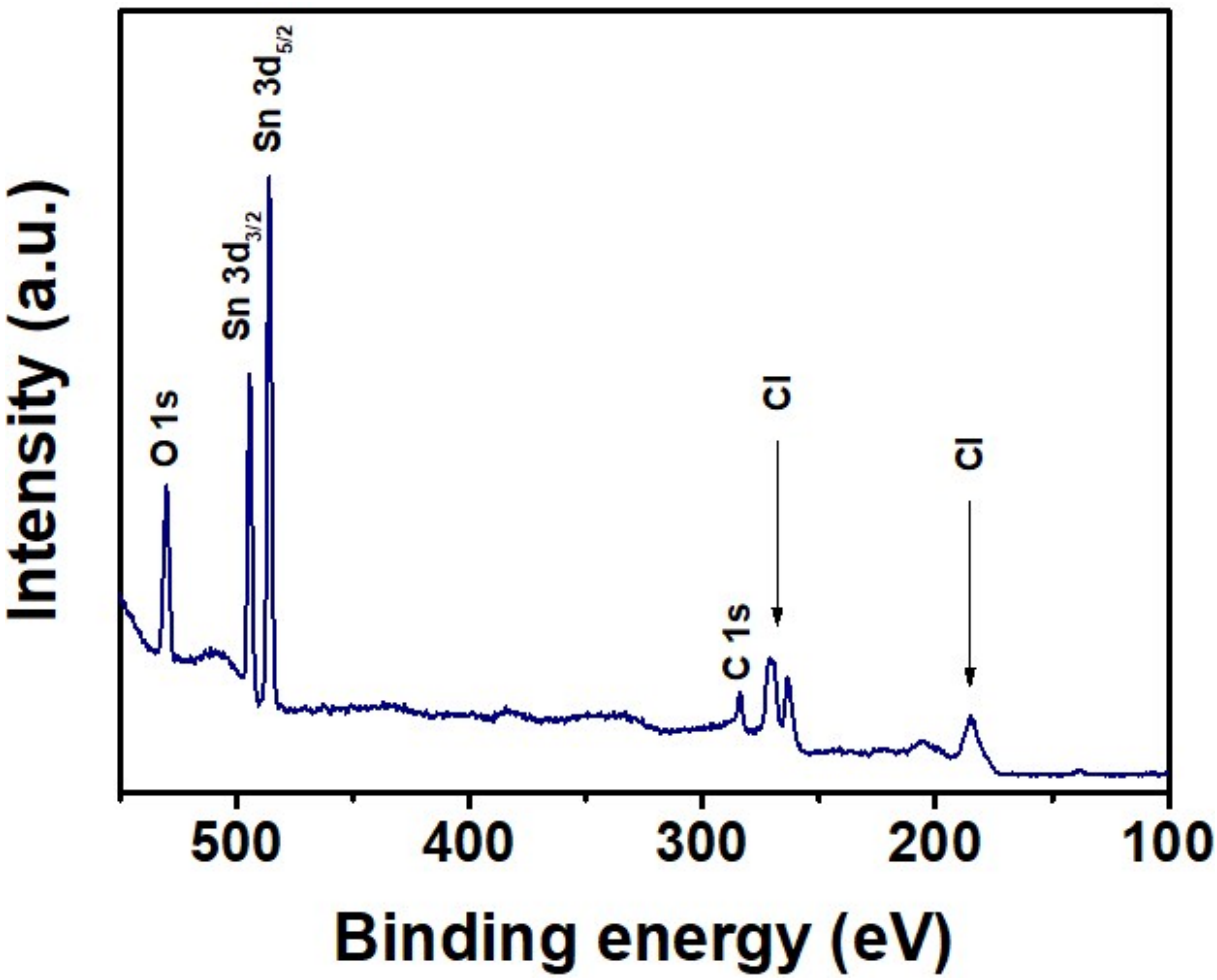

Fig. S2 XPS survey spectrum of SnO_2.

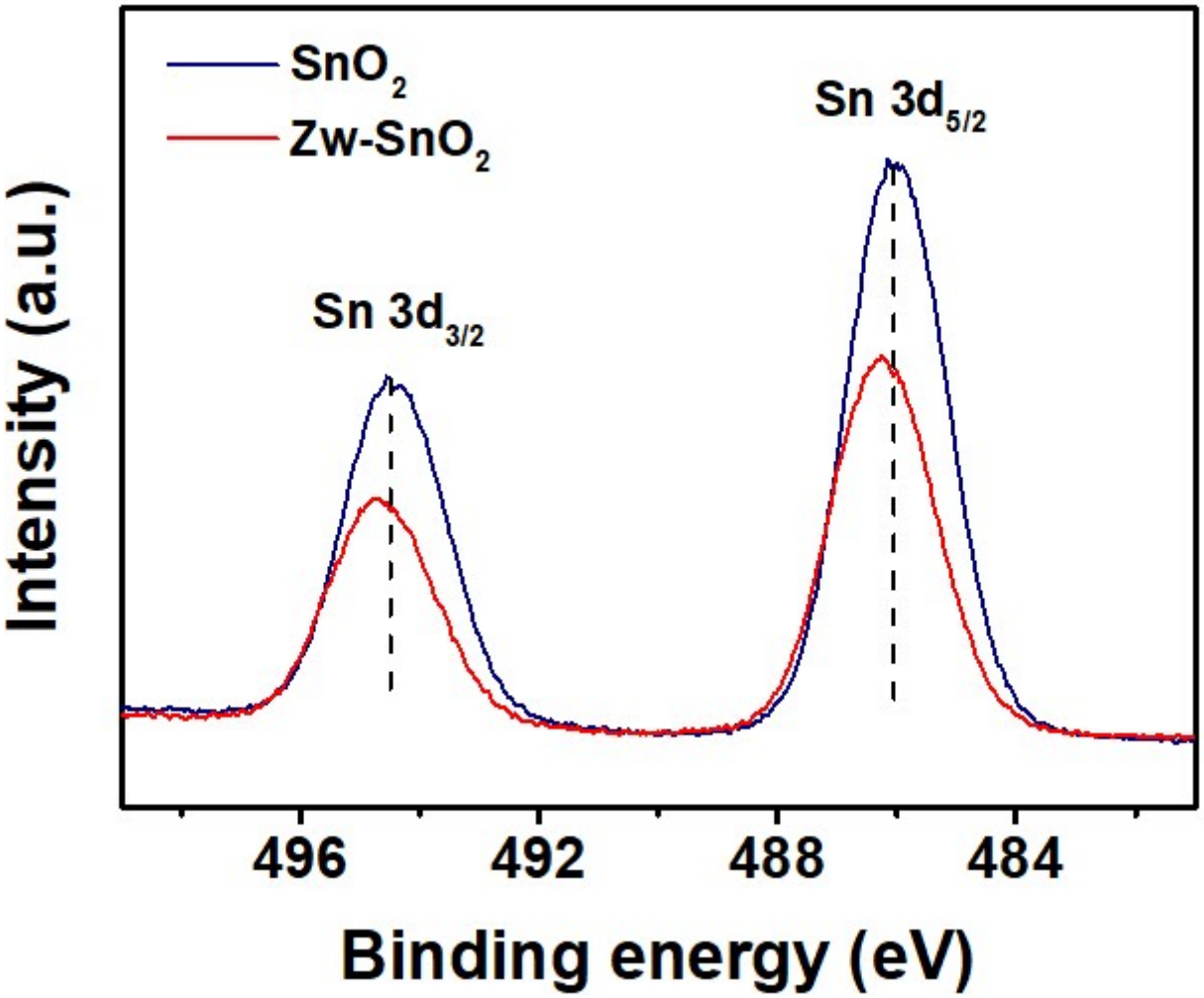

Fig. S3 XPS high resolution spectra of SnO_2 and Zw-SnO_2 for Sn 3d, respectively.

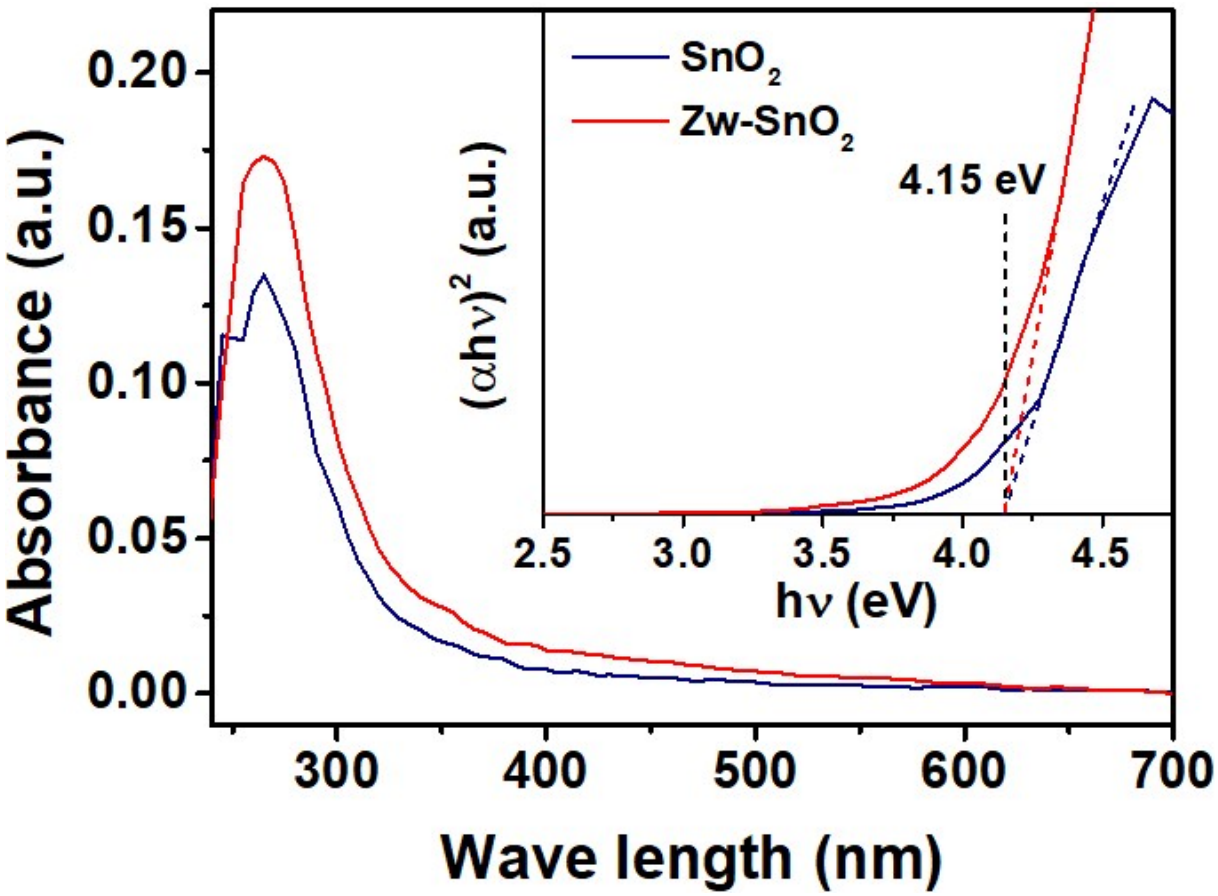

Fig. S4 Absorption spectra of SnO_2 and Zw-SnO_2, respectively. Insets: Corresponding Tauc plots for bandgap extraction.

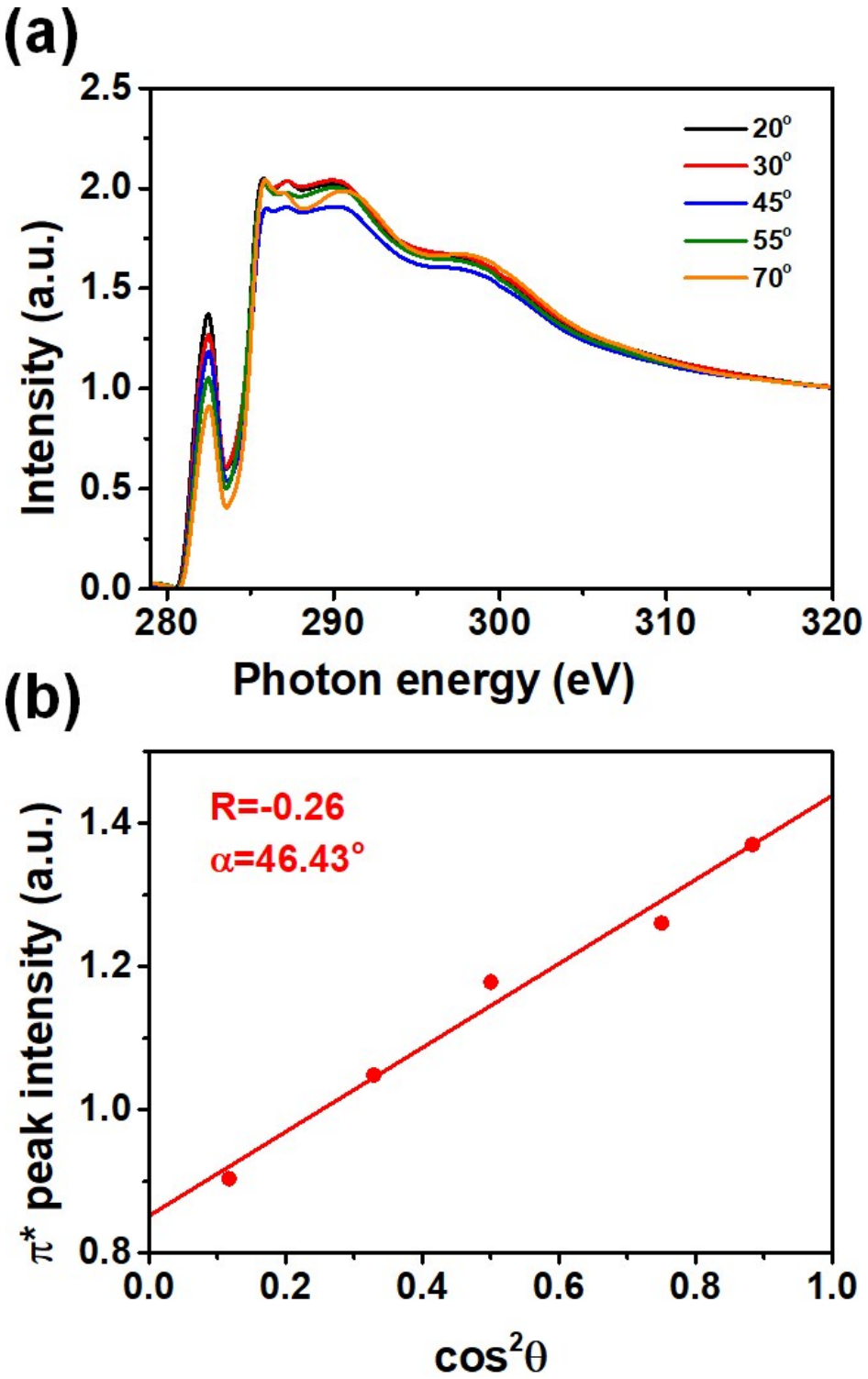

Fig. S5 (a) NEXAFS PEY mode of Zw-SnO_2. (b) Intensities of π* transitions vs incidence angle.

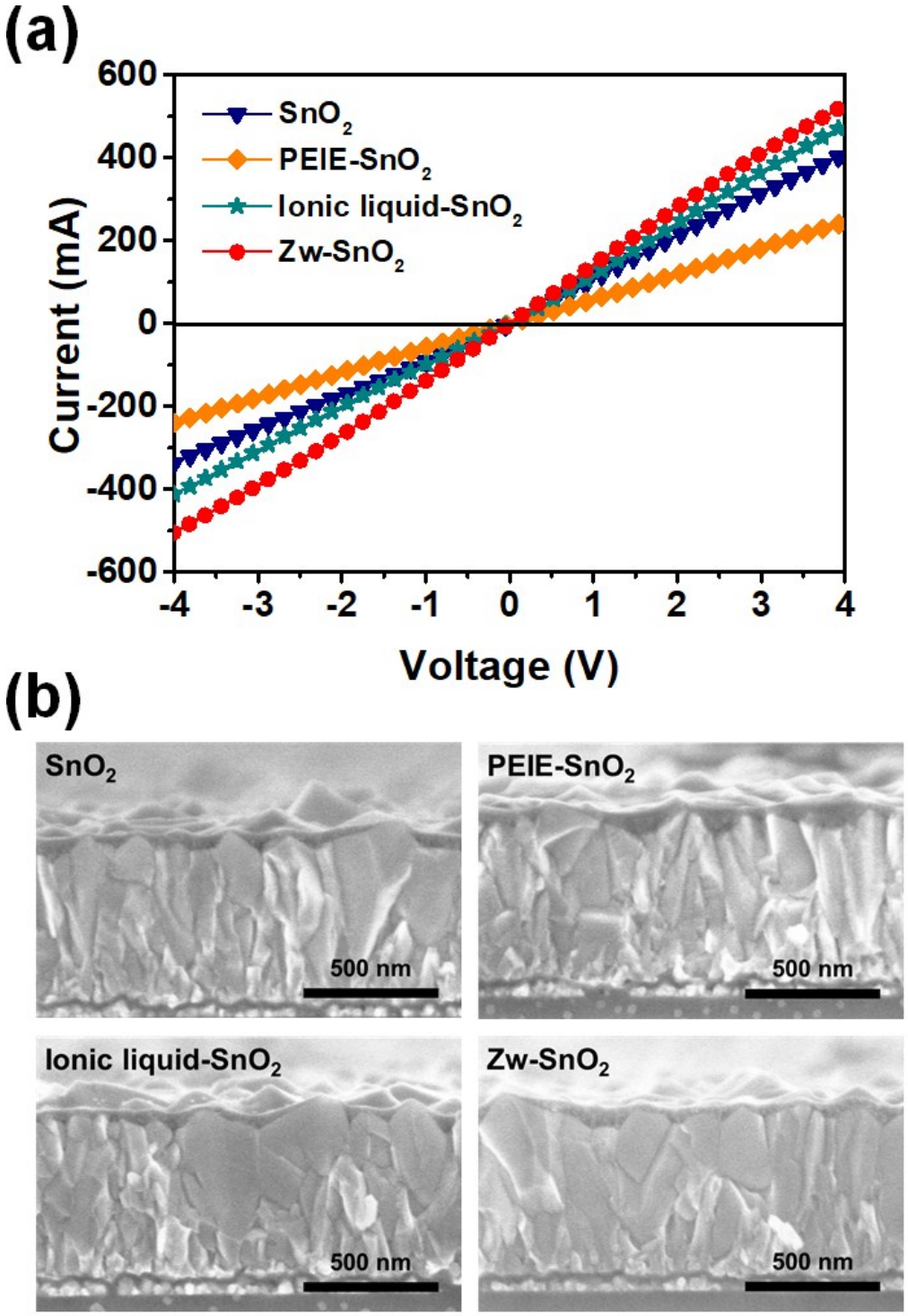

Fig. S6 (a) *I*–*V* characteristics of FTO/SnO_2/Au, FTO/SnO_2/PEIE/Au, FTO/SnO_2/IL/Au and FTO/SnO_2/zwitterion/Au devices, respectively. (b) SEM images of each ETL with different interlayers, respectively.

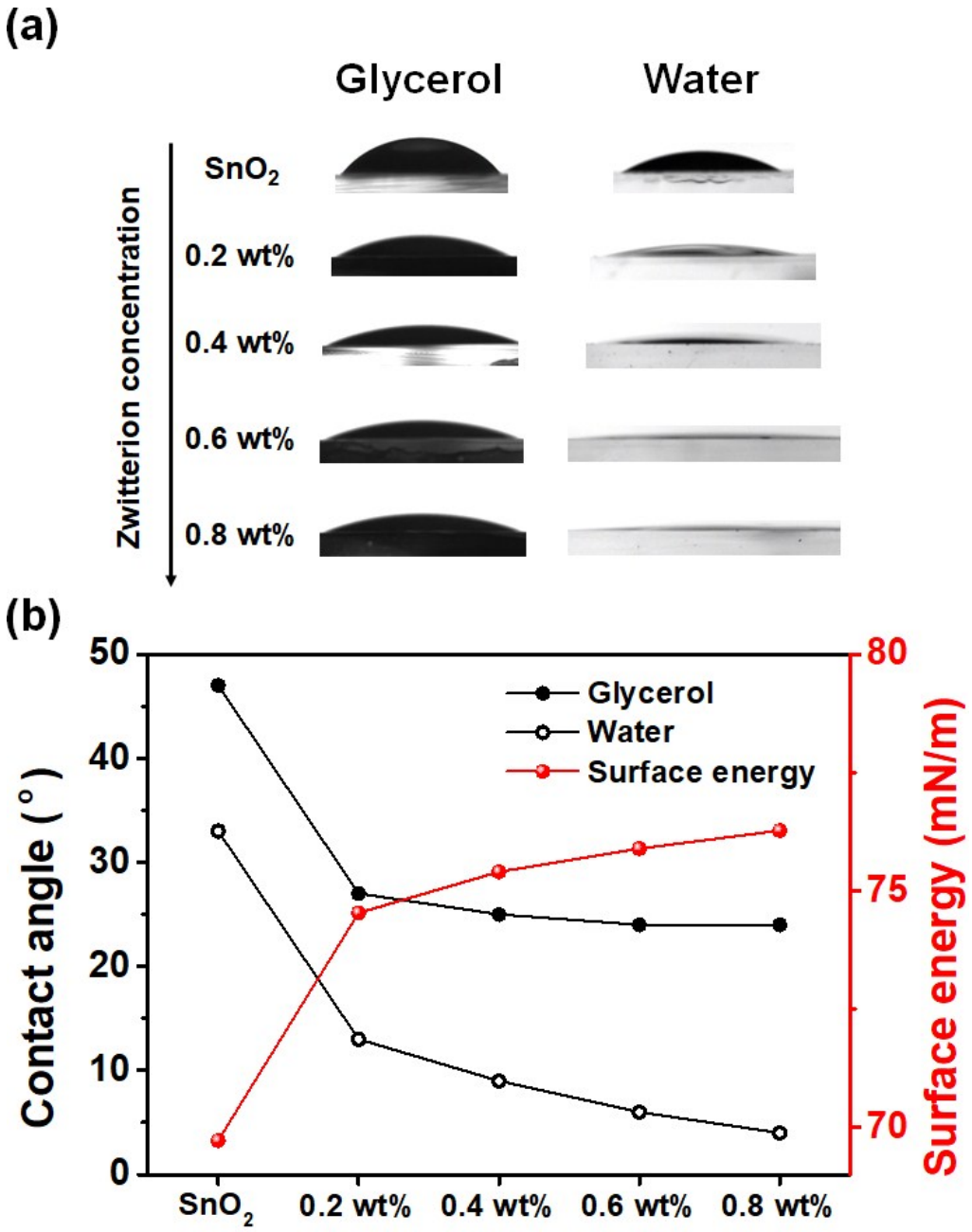

Fig. S7 (a) Contact angle images of each ETL using glycerol and DI water, respectively. (b) Contact angle values and surface energies of each ETL.

Wettability is an important factor from the viewpoint of high-quality perovskite formation because pinholes can be formed on non-wetting surfaces.[2] To confirm the surface wettability of the ETL, contact-angle measurements were performed using deionised water (DI water) and glycerol. As the amount of zwitterion increased, the contact angle decreased, and it indicates an increase in the surface energy. This result implies that wettability with the perovskite solution is improved by zwitterion modification.

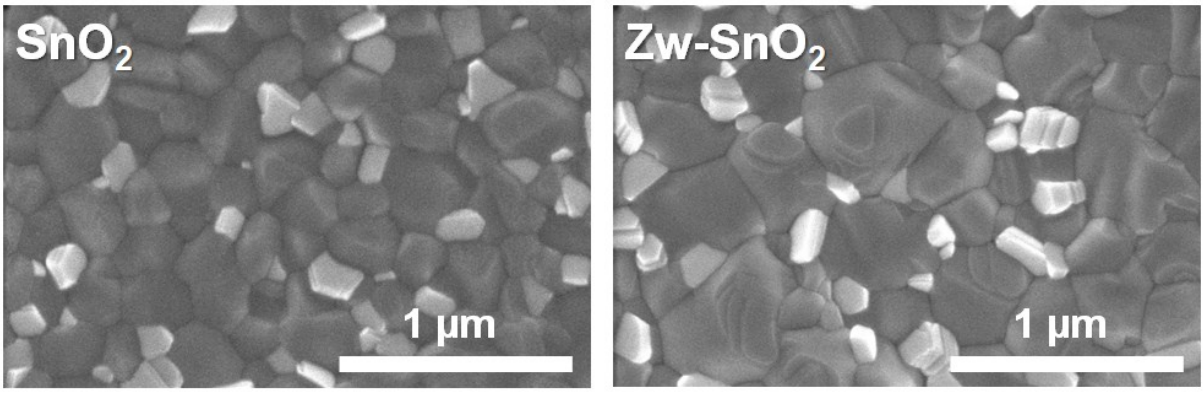

Fig. S8 Top-view SEM images of perovskite films on the SnO_2 and Zw-SnO_2, respectively.

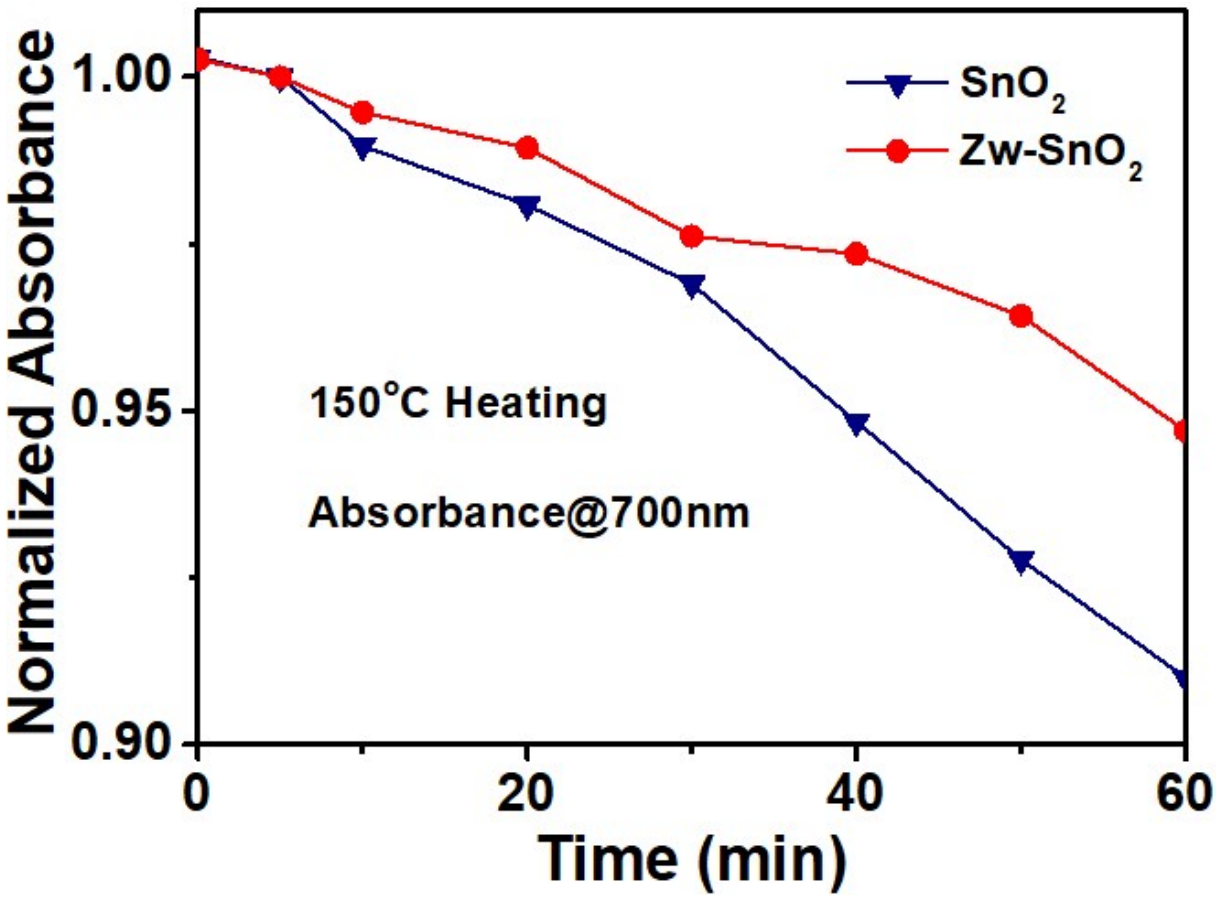

Fig. S9 Normalized absorbance at 700nm for perovskite films on the SnO_2 and Zw-SnO_2, respectively.

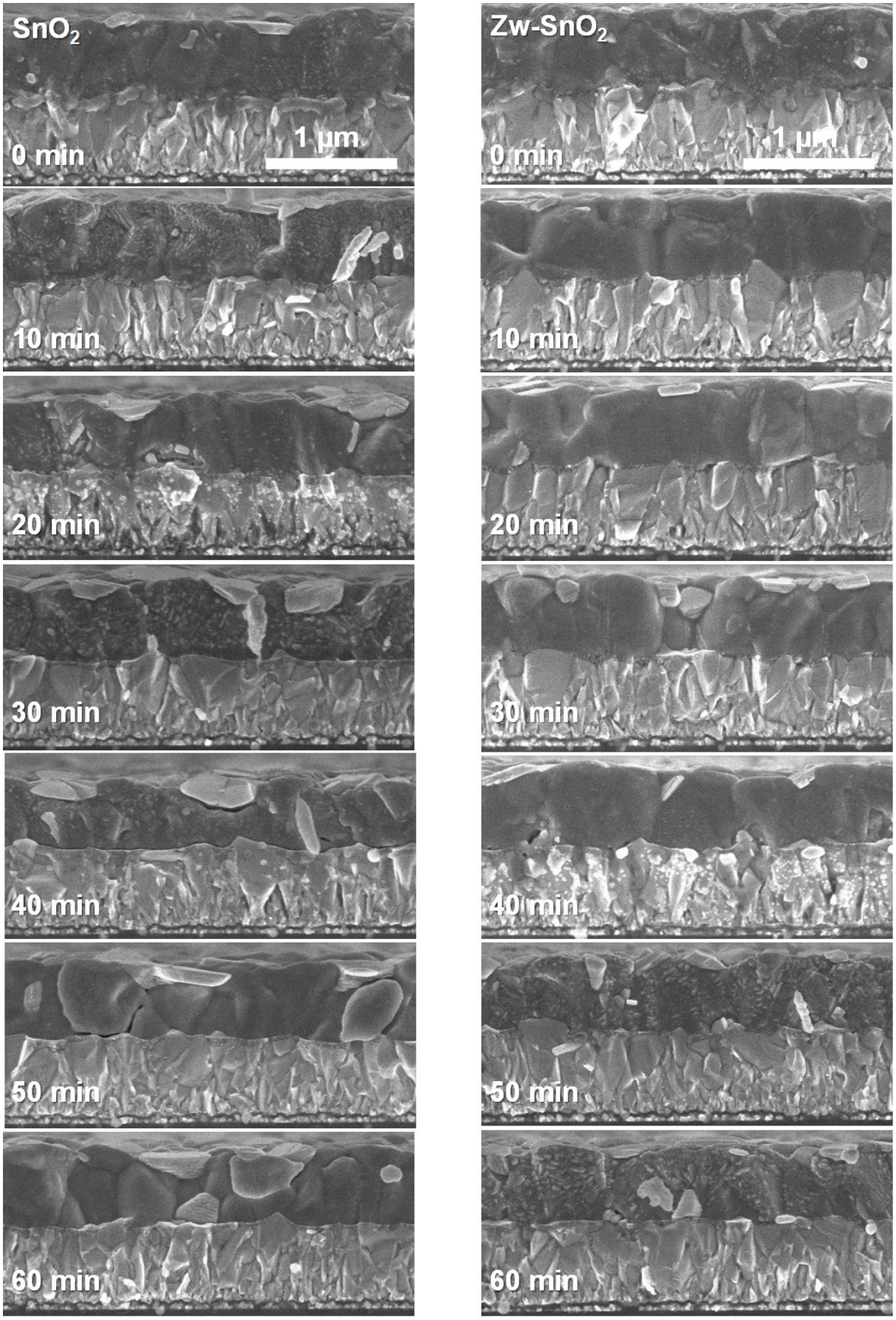

Fig. S10 Cross-sectional SEM images of the SnO_2 and Zw-SnO_2-based samples under heat treatment at 150°C.

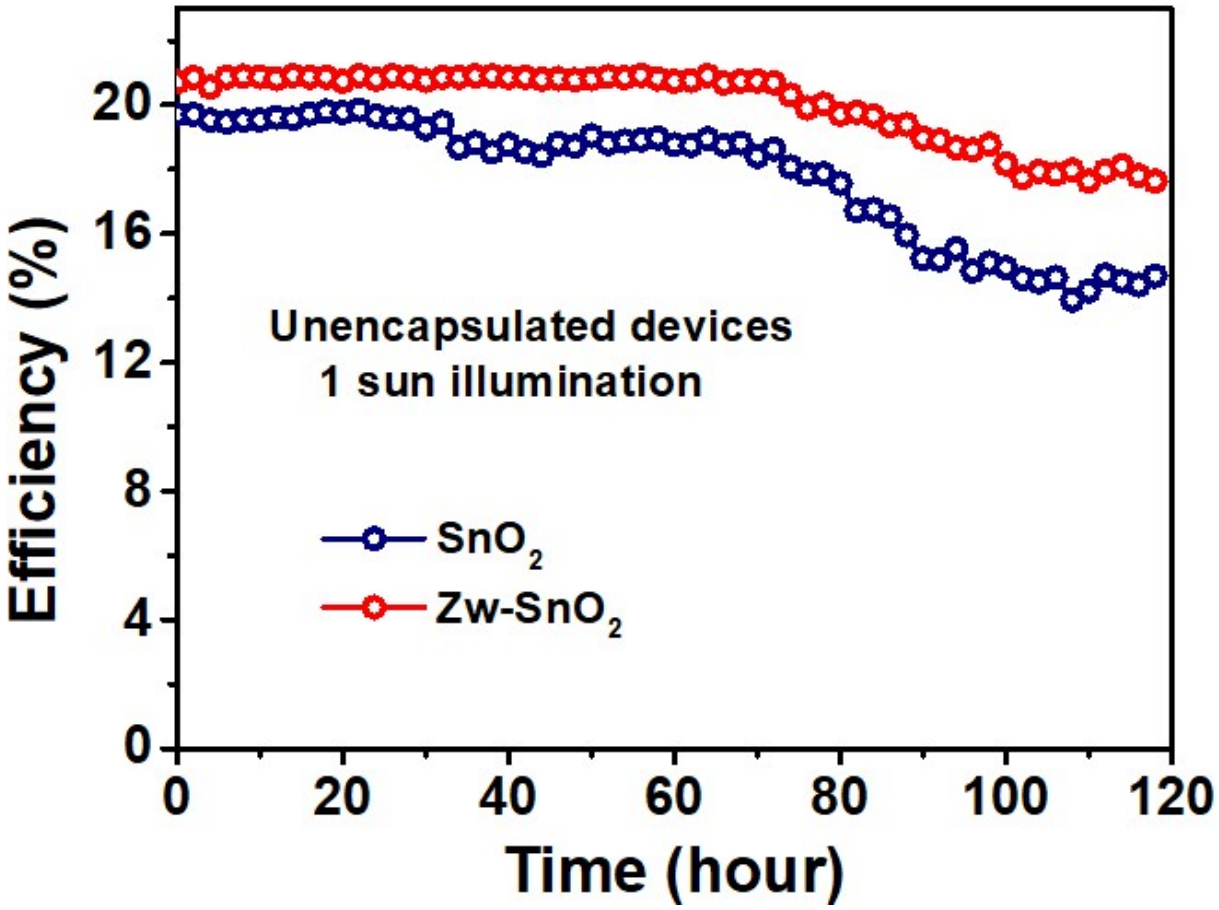

Fig. S11 PCE of the SnO_2 and Zw-SnO_2-based device as a function of time under 1 sun illumination.

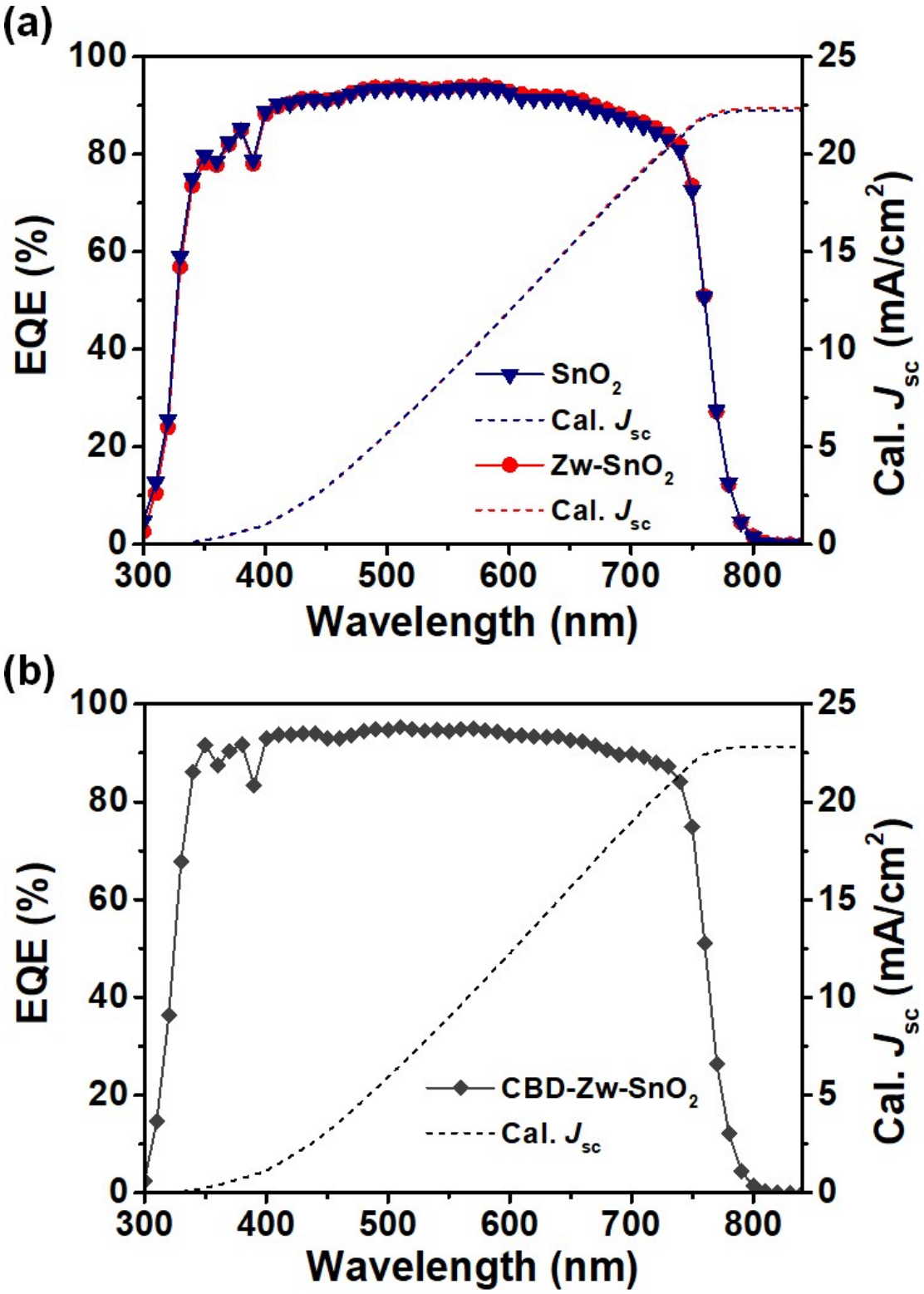

Fig. S12 IPCE measurement and integrated J_{SC} of (a) SnO_2, Zw-SnO_2 and (b) CBD-Zw-SnO_2 device, respectively.

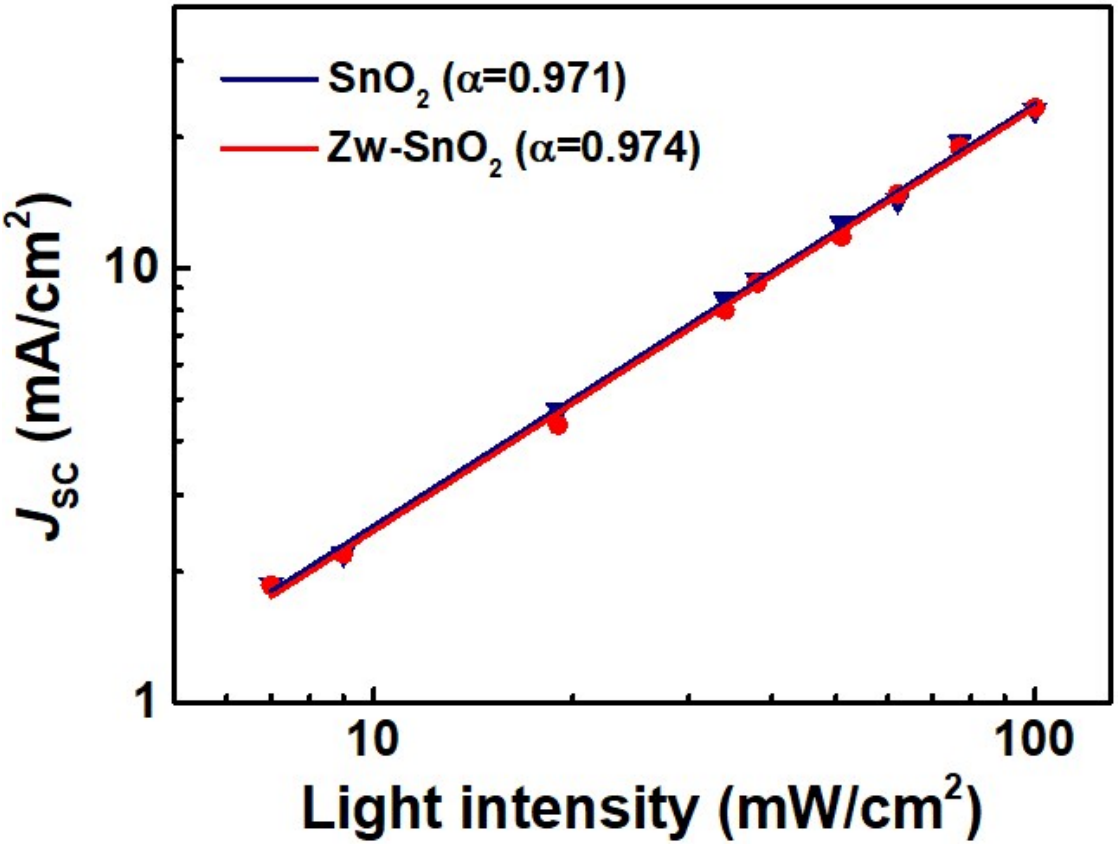

Fig. S13 J_{SC} dependence on light intensity.

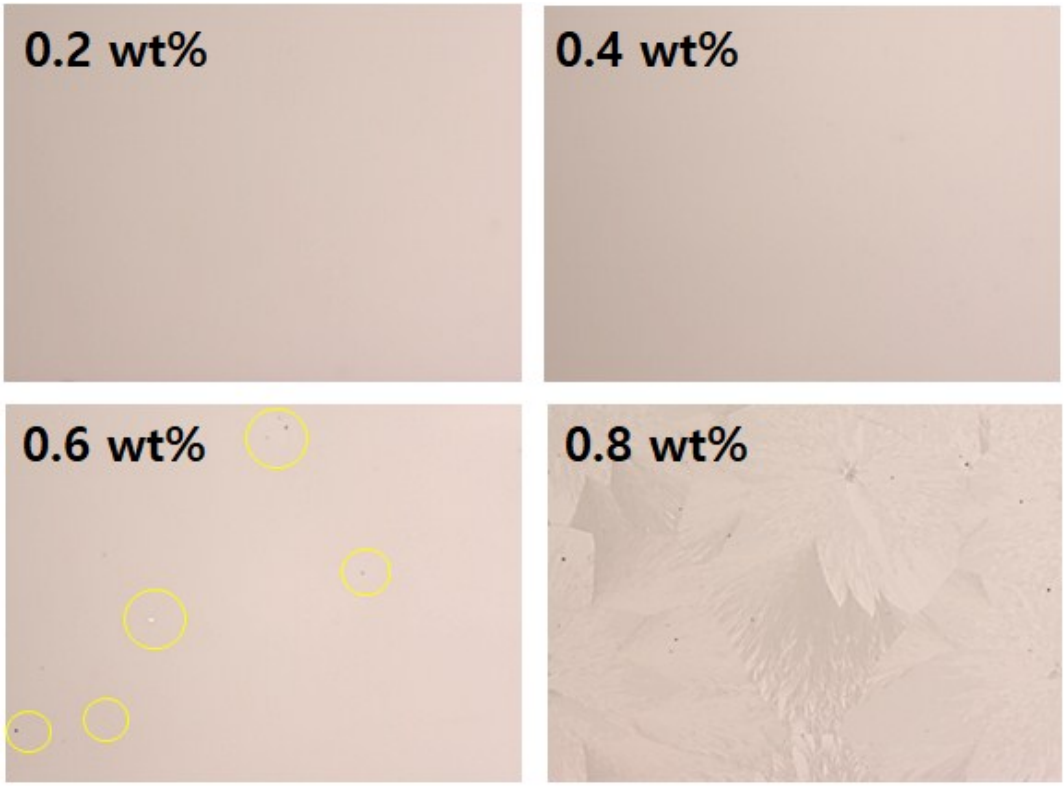

Fig. S14 Optical microscope images of Zw-SnO_2 with different concentrations, respectively.

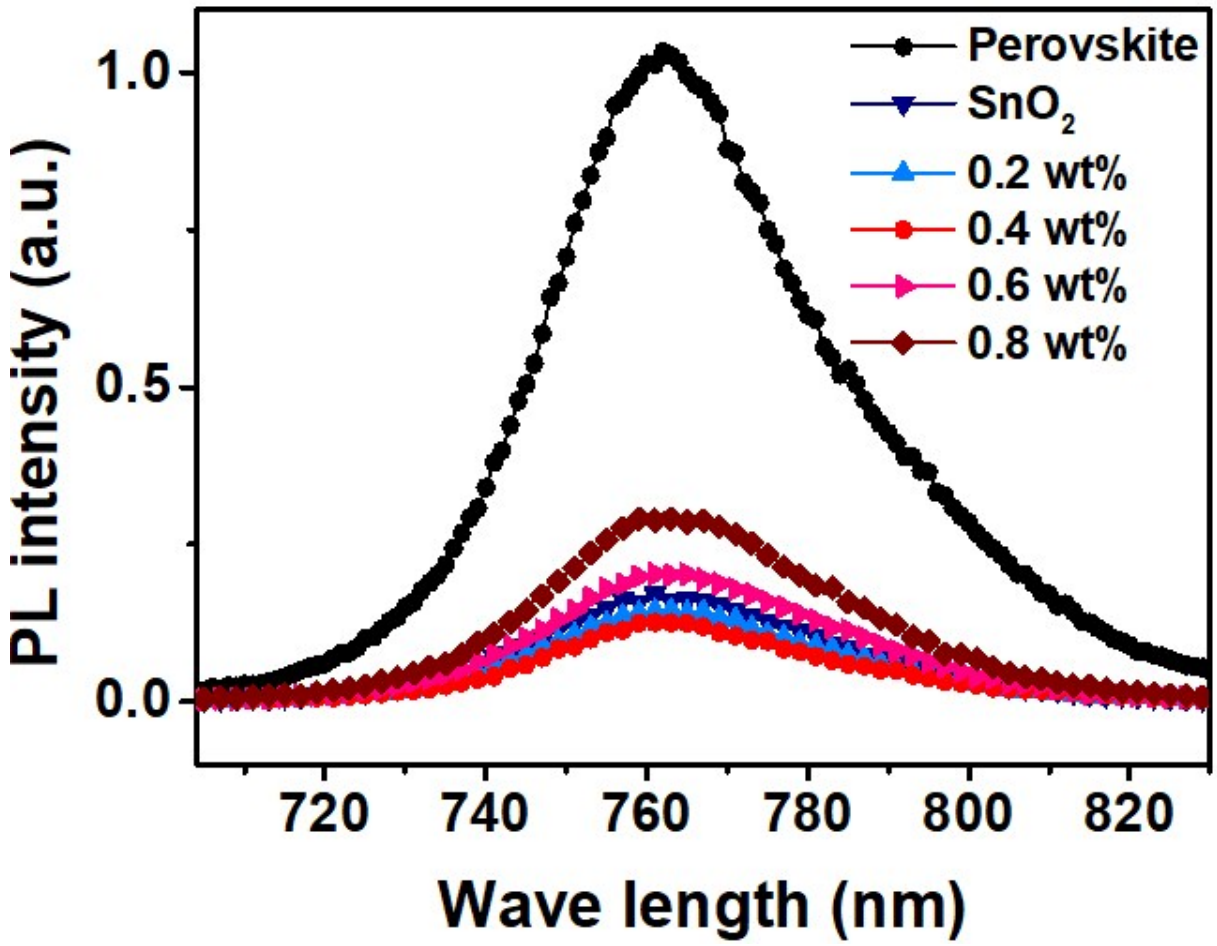

Fig. S15 Steady state photoluminescence (PL) spectra of SnO_2 and Zw-SnO_2, respectively.

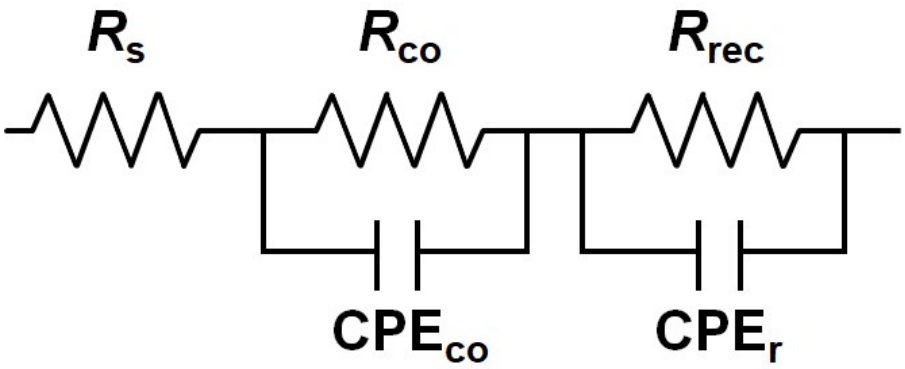

Fig. S16 Equivalent circuit model for EIS measurement.

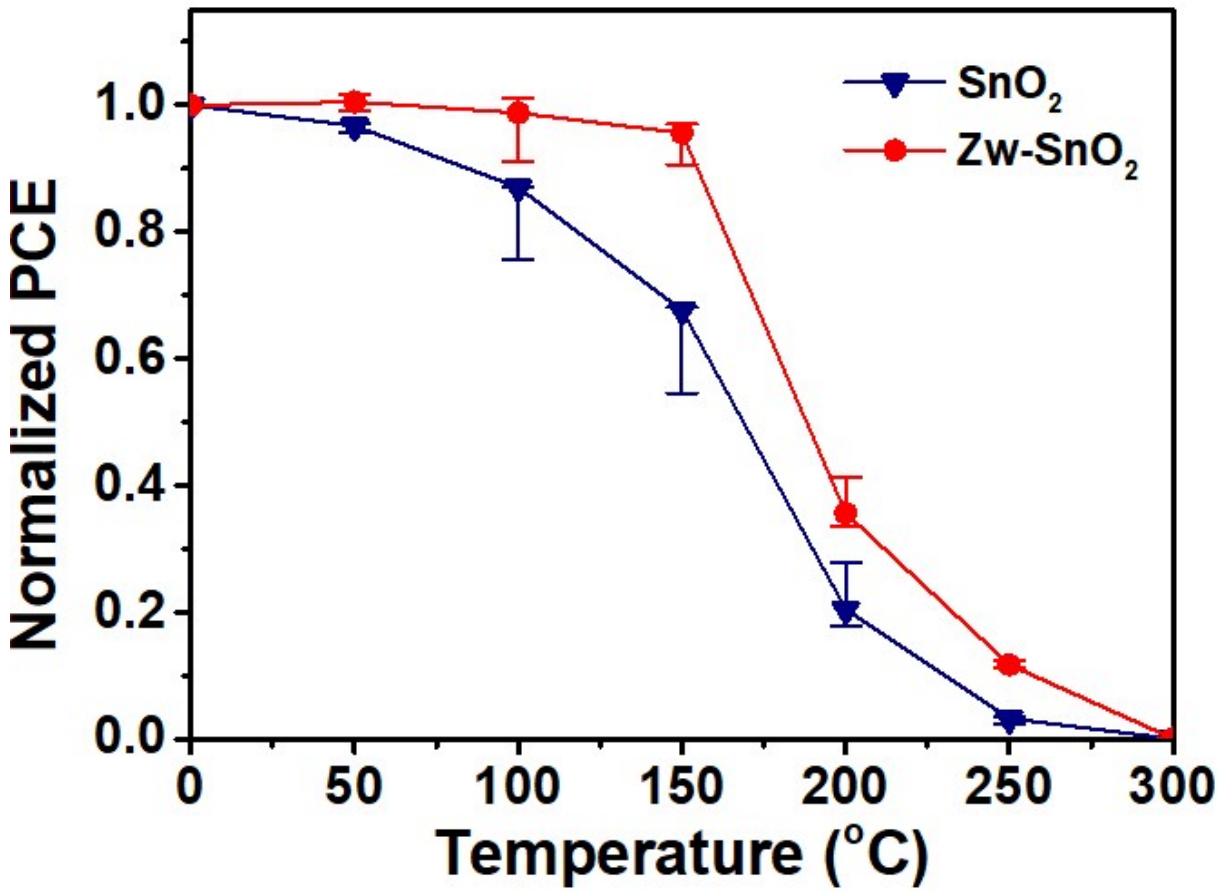

Fig. S17 Temperature-dependent thermal stability of SnO_2 and Zw-SnO_2-based devices, respectively.

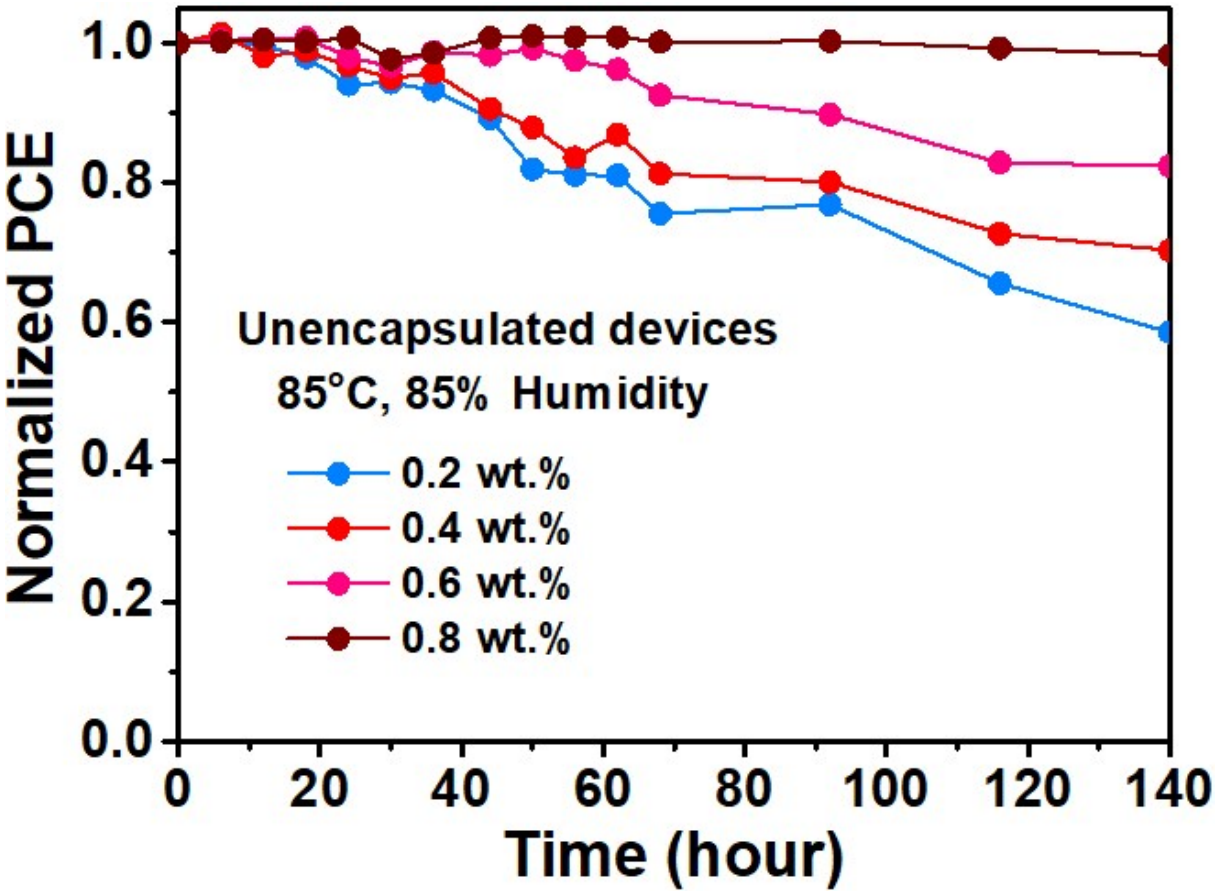

Fig. S18 Time-dependent thermal stability of device based on different concentrations of zwitterion at 85°C, 85 % humidity.

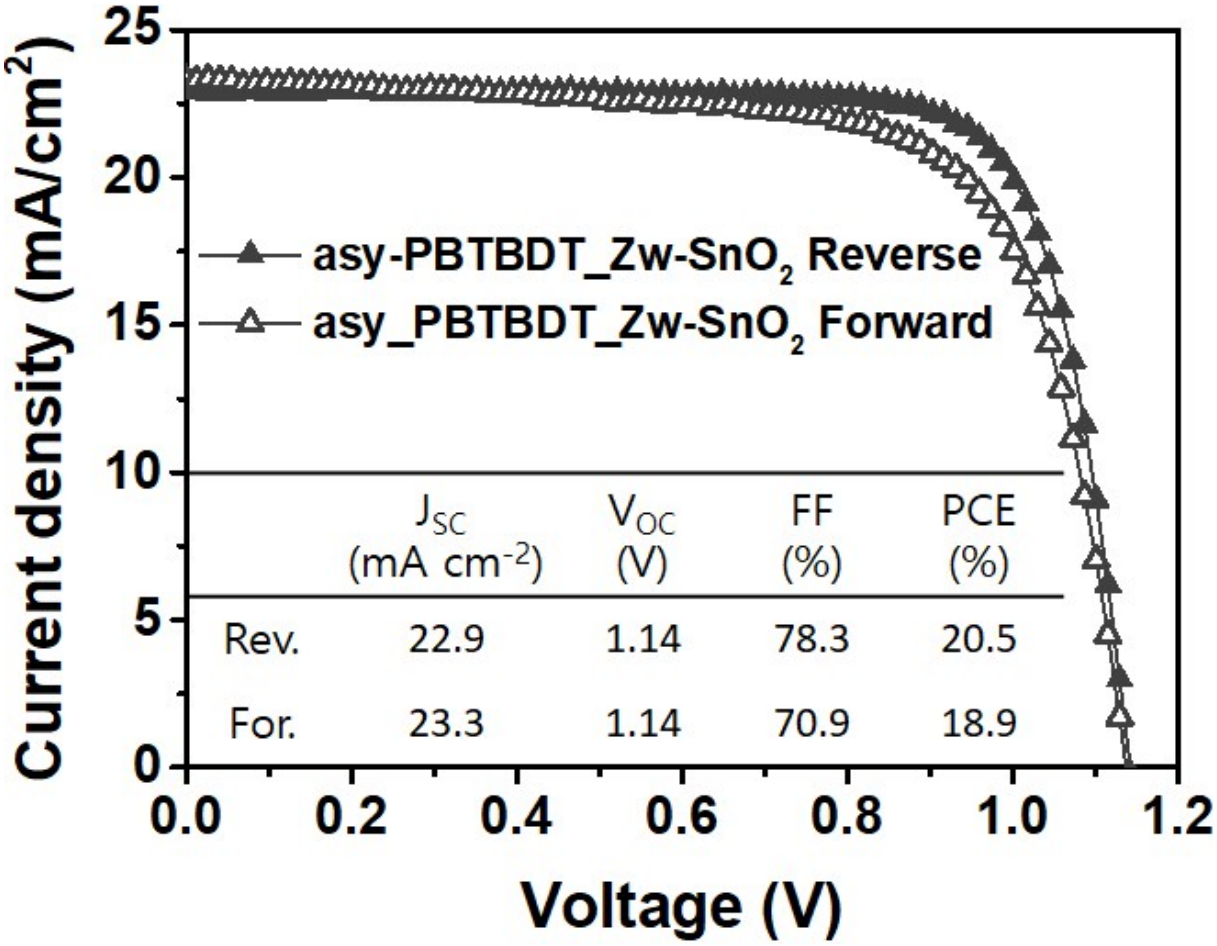

Fig. S19 *J*−*V* curves of asy_PBTBDT_Zw-SnO2-based device.

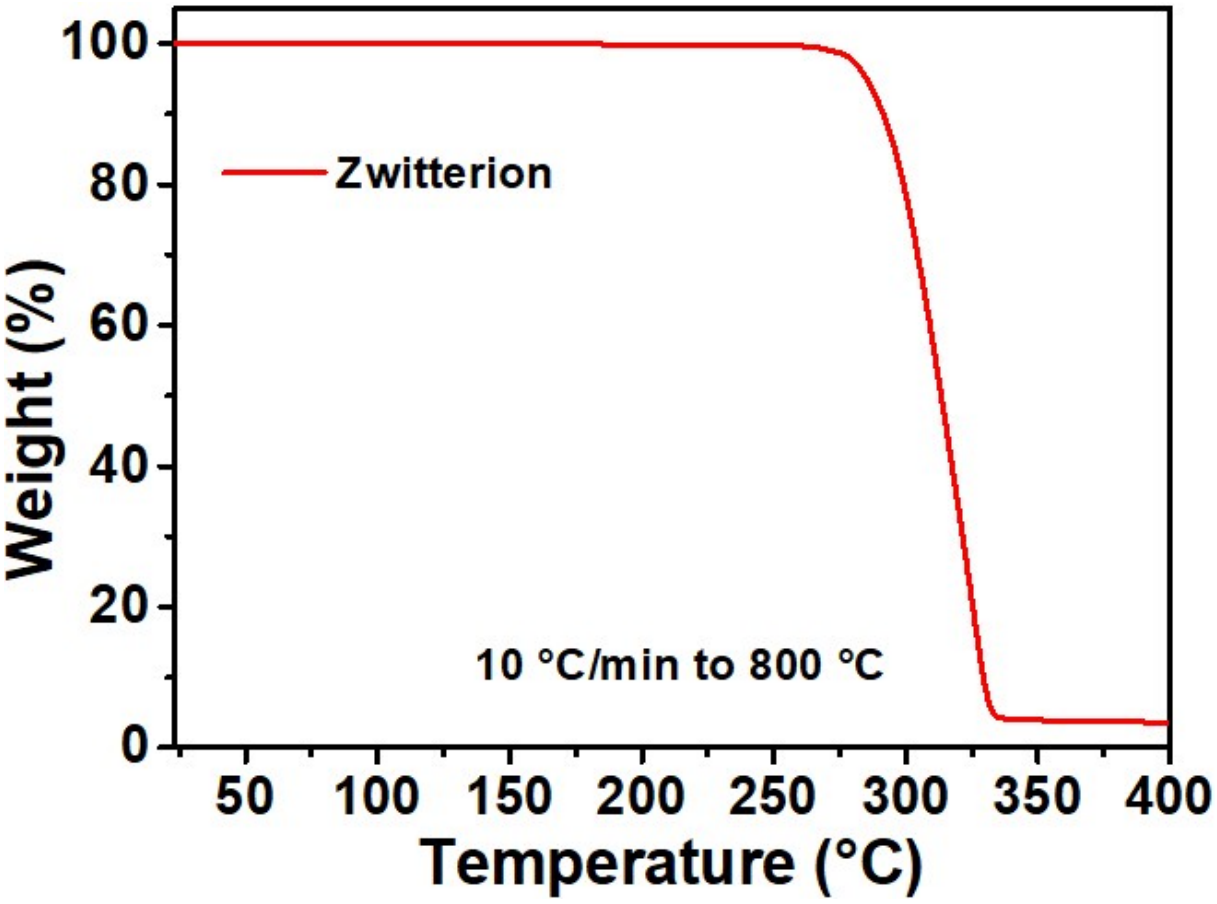

Fig. S20 TGA curve of 3-(1-pyridinio)-1-propanesulfonate.

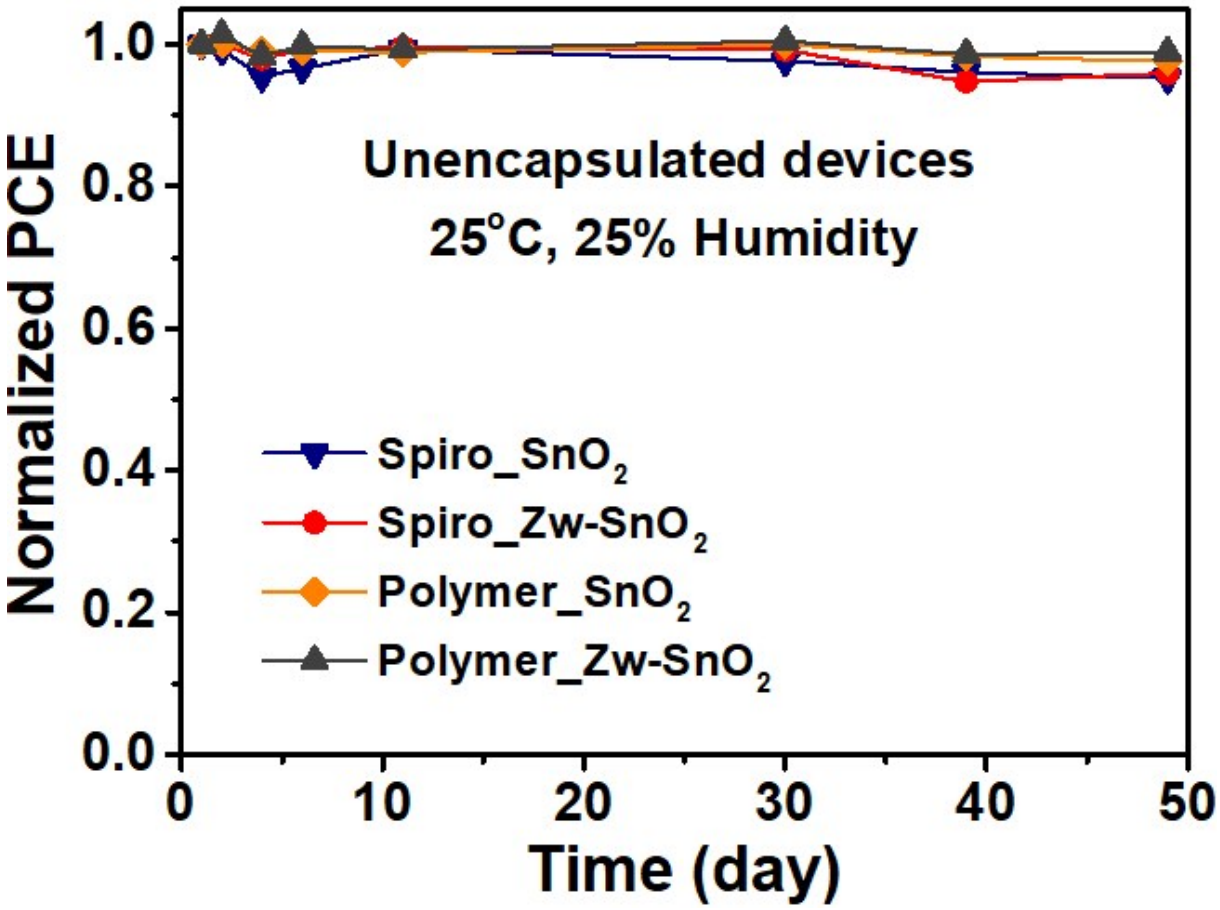

Fig. S21 Long-term stability test at 25°C, 25 % humidity.

Table S1 Calculated parameters for the energy level of ETLs

ETL	E_{cutoff} (eV)	E_{onset} (eV)	WF (eV)	E_g	VB (eV)	CB (eV)
SnO_2	16.88	4.09	4.34	4.15	8.43	4.28
Zw-SnO_2	16.99	4.14	4.23	4.15	8.37	4.22

Table S2 Calculated conductivities of each ETL with the different interlayers

ETL	Slope (I/V)	Thickness (nm)	Conductivity (mS/cm)
SnO_2	93.98	≈ 40	4.18×10^{-3}
PEIE-SnO_2	58.28	≈ 50	3.24×10^{-3}
Ionic liquid-SnO_2	110.49	≈ 40	4.91×10^{-3}
Zw-SnO_2	129.32	≈ 40	5.75×10^{-3}

Table S3 Photovoltaic parameters obtained from the best devices at each condition

ETL	J_{SC} (mA/cm^2)	V_{OC} (V)	*FF* (%)	PCE (%)
SnO_2	23.0	1.10	77.6	19.63
0.2 wt.%	23.2	1.12	78.3	20.28
0.4 wt.%	23.2	1.14	78.8	20.91
0.6 wt.%	23.1	1.13	76.0	19.90
0.8 wt.%	22.6	1.13	76.0	19.35

Table S4 Summary of the electron lifetimes

ETL	τ_1 (ns)	τ_2 (ns)	A_1 (%)	A_2 (%)
SnO_2	8.44	249.15	41.65	45.49
0.2 wt.%	8.86	169.18	51.01	37.49
0.4 wt.%	5.86	131.71	54.13	40.03
0.6 wt.%	9.01	317.64	46.09	48.09
0.8 wt.%	11.35	445.74	43.82	45.18

Table S5 Slope of the Mott–Schottky plots and doping densities of ETLs

ETL	Slope ($10^{16} \times F^{-2} V^{-1}$)	N ($10^{15} \times cm^{-3}$)
SnO_2	10.08	4.38
0.2 wt.%	7.38	5.99
0.4 wt.%	6.76	6.53
0.6 wt.%	5.31	8.31
0.8 wt.%	4.67	9.45

Table S6 Parameters of the equivalent circuit

ETL	R_s (Ω)	R_{rec} (Ω)
SnO_2	8.00	133
Zw-SnO_2	8.10	255

Table S7 The initial absolute PCEs for SnO_2 and Zw-SnO2 devices

SnO_2				Zw-SnO_2			
J_{SC} (mA cm^{-2})	V_{OC} (V)	*FF* (%)	PCE (%)	J_{SC} (mA cm^{-2})	V_{OC} (V)	*FF* (%)	PCE (%)
23	1.12	76.4	19.59	22.8	1.17	77.7	20.74
22.9	1.09	76	18.91	23.1	1.17	75.6	20.5
22.4	1.1	77.6	19.17	23.4	1.19	74.9	20.79
21.9	1.12	78.6	19.18	22.3	1.17	77.8	20.33
23	1.09	75.6	18.91	22.5	1.16	79.9	20.81
22.7	1.1	73.6	18.4	22.8	1.17	78.1	20.92
22.1	1.1	76.8	18.72	22.5	1.17	78.9	20.86
21.9	1.1	77.4	18.71	23.1	1.16	78.4	20.93
22.4	1.12	76.6	19.11	23	1.14	77.2	20.28
22.7	1.07	74.3	18.12	23.4	1.16	77.1	20.97
23	1.09	75.8	18.94	23.6	1.16	76.9	21.12
22.5	1.09	77.3	18.89	23.5	1.16	75.2	20.45
23	1.07	75.9	18.71	23	1.16	77.4	20.73
23.1	1.12	74.9	19.25	22.7	1.16	77.4	20.47
22.8	1.07	78.3	19.02	22.8	1.16	79.5	20.98
23	1.07	76.3	18.71	23.2	1.17	76.7	20.88
23.1	1.05	75.6	18.39	22.6	1.17	79.5	21.06
22.5	1.09	76.2	18.67	23.4	1.14	75.8	20.25

Table S8 Summary of device performances obtained from devices employing Spiro_SnO_2, Spiro_Zw-SnO_2, Polymer_SnO_2 and Polymer_Zw-SnO_2. All measurements were performed under 1 sun illumination (AM 1.5G, 100 mW cm^{-2}) and an active area of 0.09 cm^2

Structure	J_{SC} (mA cm^{-2})	V_{OC} (V)	*FF* (%)	PCE (%)
Spiro_SnO_2	22.9	1.12	77.5	19.8
After 140 h	19.9	0.948	45.8	8.6
Spiro_Zw-SnO_2	22.9	1.16	79.7	21.1
After 140 h	21.7	1.07	63.6	14.8
Polymer_SnO_2	22.2	1.1	77.1	18.8
After 140 h	21.1	0.974	75.2	15.4
Polymer_Zw-SnO_2	22.9	1.14	78.3	20.5
After 140 h	21.9	1.13	76.7	19.0

Reference

1. P. Giannozzi, O. Andreussi, T. Brumme, O. Bunau, M. B. Nardelli, M. Calandra, R. Car, C. Cavazzoni, D. Ceresoli, M. Cococcioni, N. Colonna, I. Carnimeo, A. D. Corso, S. de Gironcoli, P. Delugas, R. A. DiStasio Jr, A. Ferretti, A. Floris, G. Fratesi, G. Fugallo, R. Gebauer, U. Gerstmann, F. Giustino, T. Gorni, J. Jia, M. Kawamura, H.-Y. Ko, A. Kokalj, E. Küçükbenli, M. Lazzeri, M. Marsili, N. Marzari, F. Mauri, N. L. Nguyen, H.-V. Nguyen, A. O.-de-la-Roza, L. Paulatto, S. Poncé, D. Rocca, R. Sabatini, B. Santra, M. Schlipf, A. P. Seitsonen, A. Smogunov, I. Timrov, T. Thonhauser, P. Umari, N. Vast, X. Wu and S. Baroni, *J. Phys.: Condens. Matter*, 2017, **29**, 465901.

2. S. Song, M. T. Hörantner, K. Choi, H. J. Snaith and T. Park, *J. Mater. Chem. A*, 2017, **5**, 3812-3818.